Da00a

NUCLEAR SCIENCE AND ENGINEERING: 134, 121–134 (2000)

Two-Dimensional Discrete Ordinates Photon Transport Calculations for Brachytherapy Dosimetry Applications

George M. Daskalov*

National Research Council of Canada, IRS/INMS, 1500 Montreal Road
Ottawa, Ontario K1A 0R6, Canada

Randal S. Baker

Los Alamos National Laboratory, Mail Stop D409, Los Alamos, New Mexico 87545

Robert C. Little

Los Alamos National Laboratory, Mail Stop F663, Los Alamos, New Mexico 87545

David W. O. Rogers

National Research Council of Canada, IRS/INMS, 1500 Montreal Road
Ottawa, Ontario K1A 0R6, Canada

and

Jeffrey F. Williamson

Washington University Medical School, Radiation Oncology Physics
510 S. Kingshighway Boulevard, St. Louis, Missouri 63110

Received February 23, 1999
Accepted June 4, 1999

Abstract—*The DANTSYS discrete ordinates computer code system is applied to quantitative estimation of water kerma rate distributions in the vicinity of discrete photon sources with energies in the 20- to 800-keV range in two-dimensional cylindrical r-z geometry. Unencapsulated sources immersed in cylindrical water phantoms of 40-cm diameter and 40-cm height are modeled in either homogeneous phantoms or shielded by Ti, Fe, and Pb filters with thicknesses of 1 and 2 mean free paths. The obtained dose results are compared with corresponding photon Monte Carlo simulations. A 210-group photon cross-section library for applications in this energy range is developed and applied, together with a general-purpose 42-group library developed at Los Alamos National Laboratory, for DANTSYS calculations. The accuracy of DANTSYS with the 42-group library relative to Monte Carlo exhibits large pointwise fluctuations from −42 to +84%. The major cause for the observed discrepancies is determined to be the inadequacy of the weighting function used for the 42-group library derivation. DANTSYS simulations with a finer 210-group library show excellent accuracy on and off the source transverse plane relative to Monte Carlo kerma calculations, varying from −4.9 to 3.7%. The P_3 Legendre polynomial expansion of the angular scattering function is shown to be sufficient for accurate calculations. The results demonstrate that DANTSYS is capable of calculating photon doses in very good agreement with Monte Carlo and that the multigroup cross-section library and efficient techniques for mitigation of ray effects are critical for accurate discrete ordinates implementation.*

*E-mail: daskalov@irs.phy.nrc.ca

I. INTRODUCTION

Brachytherapy, or the implantation in or near localized tumors of photon-emitting sealed sources (e.g., containing isotopes such as ^{137}Cs, ^{192}Ir, or ^{125}I, which emit photons with energies below 800 keV), is widely used in cancer treatment. Currently, brachytherapy dose distributions are calculated by summing the dose contributions at each point of interest from precalculated single-source dose arrays. These algorithms assume that the sources are implanted in a homogeneous water medium and ignore source-to-source attenuation, applicator attenuation, shielding effects, and the influence of tissue heterogeneities.[1] As these effects are known[1,2] to significantly perturb the administered dose distribution, there is an urgent need to develop more accurate dose calculation algorithms that are valid near tissue and applicator heterogeneities. Such an algorithm should have accuracy of the order of 5% and be able to calculate the dose distributions within complex heterogeneous geometries over a fine three-dimensional grid in no more than a few hours. Currently, the Monte Carlo method is the only computational method satisfying this accuracy criterion.[1–3] However, its practical application to brachytherapy treatment planning is limited because of the long computational times required.

The discrete ordinates method[4] is, in principle, as accurate as Monte Carlo and has the potential to provide three-dimensional detailed flux and kerma distributions faster than the corresponding Monte Carlo simulations. Discrete ordinates calculations have been extensively benchmarked against Monte Carlo, analytical benchmarks, and measurements—mostly for neutron application.[5–7] Most of the photon transport applications that have been reported are confined either to the transport of a secondary gamma flux arising from neutron interactions (e.g., Refs. 5 and 6) or to buildup factor determination for kernel-shielding calculations.[8–11] A few reported studies include two- and three-dimensional discrete ordinates modeling of gamma-ray exposure rates due to ^{60}Co (~1.25 MeV) or higher energies through complex shielding elements,[12,13] or in air-ground geometry,[14] and show marginal (within a factor of 2) accuracy. To our knowledge, discrete ordinates methods have never been applied in multidimensional geometries for modeling the dosimetry properties of small sources emitting photons with energies below 800 keV and embedded in a shallow penetration medium.

The present study is a continuation of our work presented at the 1998 American Nuclear Society Topical Conference in Nashville, Tennessee.[15] Our aims are

1. to evaluate the accuracy of discrete ordinates water-kerma estimates relative to Monte Carlo simulations for sources with dimensions and photon spectra characteristic of brachytherapy
2. to identify the necessary conditions and computational parameters for a production-oriented discrete ordinates code that are needed to achieve the accuracy of 5% or better required for clinical applications
3. to develop a multigroup cross-section library suitable for brachytherapy discrete ordinates calculations and assess its applicability and potential limitations.

We have employed the DANTSYS standard production multigroup discrete ordinates code system[16] to evaluate the accuracy of its photon kerma calculations in two-dimensional cylindrical geometries for photon emitters with energies below 800 keV, using continuous-energy Monte Carlo calculations as benchmarks. Coherent and incoherent scattering, along with the photoeffect, are the prevalent photon interaction processes in this energy range. Because of the photoeffect, the total interaction cross section varies rapidly with energy, in particular below 100 keV, and changes significantly with the atomic number of the medium.

II. MATERIALS AND METHODS

II.A. Overall Method and Description of the Computational Benchmark Problems

We have used both DANTSYS (Ref. 16) and a continuous-energy Monte Carlo Photon Transport (MCPT) code[2,17–20] to evaluate the water kerma at various points in cylindrical water phantoms of 40-cm diameter and 40-cm height. The Monte Carlo results are then used as a "gold standard" to evaluate the accuracy of the corresponding DANTSYS calculations. A broad-energy 42-group cross-section library together with a fine-energy 210-group library specifically developed for this study have been used for all DANTSYS calculations. A detailed discussion of the cross-section data used is given in Sec. II.B. The DANTSYS and Monte Carlo computational details are discussed in Secs. II.C and II.D, respectively.

Figure 1 shows the principal geometry of the computational benchmark problems. Cylindrical volume sources of diameter d and height h are located at the center of a water phantom. The source volume is assumed to have a diameter $d = 0.05$ cm and height $h = 0.3$ cm for average source photon energies below 400 keV, and $d = 0.1$ cm and $h = 1.4$ cm for energies above 400 keV. These dimensions are characteristic of brachytherapy clinical sources. The Monte Carlo kerma estimator points have been distributed in the transverse plane bisecting the source at distances from 0.2 to 10 cm. Additional sets of estimator points have been distributed along spherical surfaces centered at the source volume center of radii $r = 1.5$, 5.0, and 10.0 cm, as shown in Fig. 1. The angles θ with the positive z-axis direction have been in the range 0 to 90 deg. We have also used elemental titanium, iron,

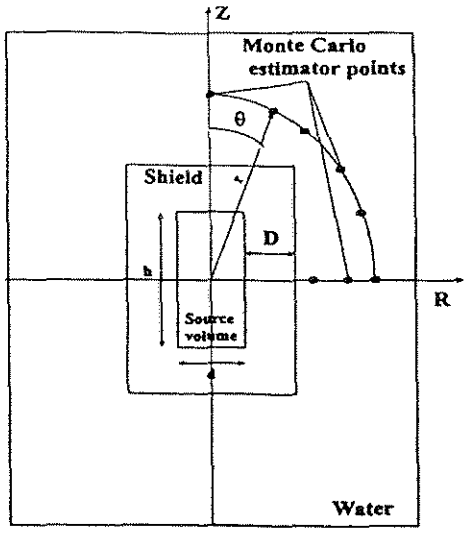

Fig. 1. Schematic of the benchmark problems. The shield material may be Ti, Fe, or Pb or may be absent in the homogeneous case.

and lead cylindrical shielding shells of thicknesses D equal to 1 and 2 mean free paths (mfp) surrounding the simulated sources and resulting in a 36 and 13% primary photon transmission factor, respectively, to analyze the filtered kerma. Along with water, these materials have been chosen because their cross sections are representative of the low-, medium-, and high-atomic-number materials found in clinical brachytherapy sources. The data for 1-mfp thickness of the materials at the source energies used for our calculations are included in Table I.

Three different kinds of primary photon spectra have been used in our Monte Carlo calculations. The first kind consists of continuous spectra simulating monochromatic multigroup spectra in the intervals 30 to 45 keV (39th group of the 42-group library), 75 to 100 keV (35th group), 200 to 300 keV (32nd), and 600 to 700 keV (26th). In addition, we have also used a continuous spectrum in 30 to 45 keV with a probability density function proportional to E^2, corresponding to the weighting function below 100 keV used in the 42-group cross-section library derivation. The second kind consists of discrete monoenergetic spectra of 100, 600, and 87 keV (to assess the lead K-edge effects). The third kind includes the actual polychromatic discrete photon spectra of ^{137}Cs (Ref. 21), ^{192}Ir (Ref. 22), and ^{125}I (Ref. 21). In all cases, the sources have been assumed to be uniformly distributed in volume throughout the source region. Table I contains the list of the source spectra used along with the spectral mean energies.

II.B. Cross Sections

II.B.1. Multigroup Cross Sections

Initially, the general-purpose 42-group cross-section library developed at Los Alamos National Laboratory (referred to hereafter as GAM-42) was used as a reference. It is based on the Evaluated Photon Data Library[23] (EPDL) in the ENDF/B-VI format and was created by the NJOY code system. The library incorporates the 42-group VITAMIN-J photon energy bin structure (included as a standard feature in NJOY), which spans the energy range 1 to 50 MeV and uses a $1/E$ weighting function with rolloffs above 10 MeV and below 100 keV. GAM-42 represents the scattering cross-section coefficients as

TABLE I

Average Energies of the Various Sources and the Corresponding to 1-mfp Shield Thickness of Materials Used in Our Calculations

Source Type	Source Average Energy (keV)	Material Thickness D Corresponding to 1 mfp (cm)			
		Water $\rho = 1$ g/cm^3	Ti $\rho = 4.54$ g/cm^3	Fe $\rho = 7.874$ g/cm^3	Pb $\rho = 11.36$ g/cm^3
^{125}I	28.33	2.43	0.035	0.012	0.002
30 keV to 45 keV	37.5	3.48	0.083	0.030	0.006
30 keV to 45 keV E^2	38.68	3.59	0.083	0.003	0.006
87 keV	87.0	---	---	---	0.046
75 keV to 100 keV	87.5	5.59	0.55	0.250	0.046
100 keV	100.0	5.86	0.81	0.342	0.016
200 keV to 300 keV	250.0	7.83	---	1.030	0.150
^{192}Ir	352.92	8.93	---	1.310	0.380
600 keV	600.0	11.17	---	1.600	0.700
^{137}Cs	613.61	11.26	---	1.650	0.710
600 keV to 700 keV	650.0	11.52	---	1.650	0.800

fifth-order Legendre polynomial angular expansions. The GAM-42 library also includes the corresponding group kerma factors for converting angular flux into kerma. Except for GAM-42, all other cross-section sets are based on DLC-146 cross-section data.[24] Our assessment showed[15] that no noticeable differences are observed based on different underlying cross-section libraries (i.e., DLC-146 versus EPDL).

In developing multigroup cross-section libraries, the NJOY computer code system[25] was used. The NJOY GAMINR module[25] was employed to derive the multigroup scattering matrices incorporating the coherent and incoherent scattering cross sections important for the studied energy range. In addition, GAMINR was used to derive the corresponding multigroup heating cross sections, or kerma factors, which have been included in all developed cross-section libraries. The NJOY code was used to create a 210-group cross-section library based on DLC-146, referred to hereafter as G-210. Unlike the 148-group structure that we used previously,[15] the group energy bins span the energy range 1 keV to 1.5 MeV, thus accommodating all energies of importance in brachytherapy applications. The average energy bin widths are nonuniformly distributed over the energy range, with some groups chosen to have both boundaries coinciding with the *K*, *L*, and *M* edges of selected elements, and with an energy width <2 keV. The particular energy bin structure of G-210 is given in Table II.

The theory of the multigroup energy approach in radiation transport indicates[4] that the narrower the energy bins the less dependent are the resulting multigroup constants on the choice of the weighting function. In general, as the energy bin widths approach zero, the multigroup constants approach the corresponding pointwise values.

The G-210 cross-section library is based on a constant weighting function for all energies and angles. The corresponding flux-to-kerma group factors have been also derived and included. The G-210 scattering matrices have been expanded to allow up to fifth-order Legendre polynomial expansion of the scattering terms. The G-210 energy group structure is designed to accurately represent the photon cross sections while minimizing the choice of weighting function on the averaged group constants.

II.B.2. Continuous-Energy Cross Sections

The macroscopic cross sections used for the Monte Carlo simulations, as well as the normalized probabilities for coherent, incoherent, and photoeffect interactions, were derived from DLC-146 data[24] to avoid any systematic error due to differences in the reference data. A log-log interpolation has been performed throughout the DLC-146 energy grid to add points where necessary to achieve better than 1% accuracy when the linear interpolation procedures are employed in the continuous-energy Monte Carlo code used for the analysis.

Characteristic X-ray production following the photoeffect absorption is a significant source of secondary X rays for photons with incident energies below 300 keV in high-atomic-number materials and is an important feature in some brachytherapy applications. Accounting for the characteristic X rays is therefore a strongly desirable feature of the discrete ordinates simulations. In this study, however, since the characteristic X-ray production has not been included in the multigroup libraries developed by NJOY, it has been removed from the libraries used by the Monte Carlo code for the purpose of comparing results.

II.C. DANTSYS Calculations

The DANTSYS code package[16] is a modular computer program designed to solve the time-independent, multigroup discrete ordinates form of the linear Boltzmann transport equation in several different geometries. The TWODANT solver module solves the time-independent two-dimensional transport equation using the diamond-differencing or adaptive weighted diamond-differencing (AWDD) method[26] for space/angle discretization. Diffusion synthetic acceleration is used to accelerate convergence of the transport equation.[27]

We employed the TWODANT solver module of the DANTSYS code system for our photon transport calculations in two-dimensional cylindrical *r-z* geometry. Orders of triangular Chebychev-Legendre angular quadratures varying from 21 (S_{12}) to 465 (S_{60}) angles per octant (standard within DANTSYS) were used. Energy-dependent spatial mesh sizes <0.2 mfp along the *r*-axis were applied. In fact, the mesh sizes have been dictated by the rather small lateral dimensions of the shielding and source regions, generally resulting in <0.1-mfp step sizes. The ratio of the *z*- to *r*-axis mesh sizes (the aspect ratio) varied from 2:1 near the source volume to 35:1 at the periphery of the analyzed water phantom in the vicinity of the *r* or *z* axis. Such large aspect ratios may lead to a significant improvement in discrete ordinates calculation efficiency by reducing the number of mesh cells necessary to model the geometry. At the same time, our results show that inappropriately large aspect ratios can distort the calculated angular flux distributions by as much as 20%, relative to the Monte Carlo results.

Since the problem is symmetric with respect to the bisecting transverse source plane ($z \equiv 0$), only half of the physical space was modeled with reflection boundary conditions along $z = 0$. Reflection boundary conditions were also used along the rotational *z* axis of symmetry ($r \equiv 0$). Vacuum boundary conditions have been employed at the outer water phantom surfaces. The mesh sizes along either direction have been gradually increased with increasing average source energy. The resulting spatial mesh cell structures contained between 22 (source energies above 400 keV) and 73 (^{125}I source energy) steps along the *r* axis, and between 14 and 70 steps along the *z* axis.

A typical brachytherapy dosimetry problem consists of a nearly singular pointlike source immersed in a weakly

TABLE II

Upper Energy Boundaries of the G-210 Multigroup Cross-Section Library*

Group Number	Energy (keV)	Group Number	Energy (keV)	Group Number	Energy (keV)	Group Number	Energy (keV)	Group Number	Energy (keV)	Group Number	Energy (keV)
1	1500.00	36	325.000	71	93.0000	106	41.2500	141	29.2500	176	9.2000
2	1400.00	37	312.500	72	92.0000	107	41.0000	142	29.0000	177	8.9789
3	1340.00	38	300.000	73	91.0000	108	40.5000	143	28.7000	178	8.5000
4	1335.00	39	285.000	74	90.0000	109	40.0000	144	28.5000	179	8.3328
5	1330.00	40	275.000	75	88.0000	110	39.7500	145	28.2000	180	8.0000
6	1100.00	41	260.000	76	86.0000	111	39.5000	146	28.0000	181	7.7089
7	1000.00	42	250.000	77	83.1023	112	39.2500	147	27.6000	182	7.1120
8	950.000	43	225.000	78	80.7249	113	39.0000	148	27.2500	183	6.5390
9	900.000	44	200.000	79	77.5000	114	38.7500	149	27.0000	184	5.9892
10	850.000	45	195.000	80	76.1110	115	38.5000	150	26.2500	185	5.4651
11	825.000	46	190.000	81	69.5250	116	38.2500	151	25.5140	186	4.9664
12	800.000	47	185.000	82	65.0000	117	38.0000	152	23.7500	187	4.7500
13	780.000	48	180.000	83	60.0000	118	37.7500	153	22.5000	188	4.5000
14	750.000	49	175.000	84	57.5000	119	37.5000	154	21.2500	189	4.2500
15	735.000	50	172.500	85	55.0000	120	37.2500	155	20.0000	190	4.0000
16	720.000	51	170.000	86	53.5000	121	37.0000	156	18.9700	191	3.8510
17	700.000	52	165.000	87	52.5000	122	36.7500	157	17.9300	192	3.5540
18	690.000	53	162.500	88	51.0000	123	36.5000	158	16.9000	193	3.3100
19	680.000	54	157.000	89	50.0000	124	36.2500	159	15.8600	194	3.0660
20	665.000	55	156.000	90	48.5000	125	35.9846	160	15.2000	195	3.0000
21	635.000	56	150.000	91	47.5000	126	35.5500	161	15.0000	196	2.7930
22	620.000	57	145.000	92	46.0000	127	35.0000	162	14.8393	197	2.5860
23	600.000	58	140.000	93	45.0000	128	34.7500	163	14.3528	198	2.5350
24	597.500	59	137.500	94	44.2500	129	34.5000	164	13.8799	199	2.4840
25	595.000	60	135.000	95	44.0000	130	34.0000	165	13.4185	200	2.2420
26	575.000	61	130.000	96	43.7500	131	33.5000	166	13.0400	201	2.1210
27	550.000	62	125.000	97	43.5000	132	33.1694	167	12.8241	202	2.0000
28	500.000	63	112.500	98	43.2500	133	32.5000	168	12.2839	203	1.8750
29	450.000	64	100.000	99	43.0000	134	32.0000	169	12.0998	204	1.7500
30	400.000	65	99.0000	100	42.7500	135	31.5000	170	11.9187	205	1.6250
31	385.000	66	98.0000	101	42.5000	136	31.0000	171	11.5637	206	1.5000
32	370.000	67	97.0000	102	42.2500	137	30.5000	172	11.2154	207	1.3750
33	360.000	68	96.0000	103	42.0000	138	30.0000	173	10.7600	208	1.2500
34	350.000	69	95.0000	104	41.7500	139	29.7500	174	10.3671	209	1.1250
35	337.500	70	94.0000	105	41.5000	140	29.5000	175	9.65860	210	1.0630

*The 210th energy group lower boundary is 1 keV.

scattering medium of maximum linear dimensions of 2 to 20 mfp. These conditions are known to exacerbate artifacts inherent in the discrete ordinates method, such as ray effects. The problem is additionally aggravated by the presence of relatively thick shielding consisting of high-density absorbing materials. Our studies show that the ray effects can introduce flux aberrations as large as −32% and +76% relative to the Monte Carlo results even when 465 angles per octant are used for the calculations. These results indicate that the ray effects can completely negate the quantitative accuracy of the discrete ordinates method relative to Monte Carlo calculations. Mitigating ray effects is essential to successful application of the discrete ordinates method to brachytherapy. TWODANT's ray-tracing first-collision source option[28] was used for all DANTSYS calculations discussed here. The method uses TWODANT's internal stochastic ray-tracing algorithm to calculate the uncollided photon flux, which is thus free of any ray effects. The resulting uncollided flux is used to generate a broadly distributed first-collision source for discrete ordinates calculations of the scattered flux and the related scattering kerma. The first-collision source option allows the use of lower-order angular quadratures with a negligible impact on the accuracy. Between

365 000 and 35 000 000 ray-tracing histories were used to create the first-collision source using between 2 and 25% of the total DANTSYS CPU time. The statistical uncertainty of the uncollided flux was <3% except for mesh cells near the z-axis of rotational symmetry, where it was 3 to 30 times larger. The results and discussion in Sec. III show the relevance of the ray-tracing implementation.

The AWDD method[26] was used to eliminate negative flux fixups. The AWDD performance is controlled by the group-dependent input parameter ***wdamp***, which normally takes values between 0 and 4. A value of 0 indicates the use of the diamond-differencing scheme with a set-to-zero fixup, while a value of 4 produces a scheme heavily damped toward the step solution.[16,26] We have used ***wdamp*** = 3 for each energy group and all DANTSYS calculations since this value leads to an optimal performance during the inner iteration for all source energies. Values of ***wdamp*** other than 3 reduce the convergence rate and increase the run time by as much as 50 to 70%. In addition, values of ***wdamp*** < 1 limit aspect ratios to 3:1 to 4:1 in order to achieve sufficient accuracy of DANTSYS results relative to MCPT simulations, thus further reducing the computational efficiency.

We have used both third (P_3) and fifth (P_5) orders of Legendre polynomial expansion to model the angular dependence of the scattering matrix. The comparison between the P_5 and P_3 results (without any transport correction to the truncated scattering cross sections) shows that they closely agree and that the discrepancies do not exceed 0.5%. This result indicates that the use of P_5 approximation does not improve accuracy. The application of P_1 and P_2 orders of polynomial expansion shows pointwise fluctuations in accuracy relative to MCPT.

The iteration convergence criterion used in the DANTSYS calculations can be defined as

$$\max_{\vec{r}} |[\Phi^0_{0,g}(\vec{r})]^{k+1} - [\Phi^0_{0,g}(\vec{r})]^k| \le \epsilon_{in} \ , \qquad (1)$$

where $[\Phi^0_{0,g}(\vec{r})]^k$ is the scalar flux for group g at $\vec{r}$ after the k'th inner iteration. In all DANTSYS calculations discussed here, $\epsilon_{in} = 0.0001$.

The DANTSYS CPU running time is roughly proportional to the number of phase-space cells (energy-angle-space) used for problem discretization, provided the same P_N order of angular expansion is used. With the G-210 multigroup library, the CPU time varied between 0.1 min/spatial point (for a case of 73 × 49 spatial cells, ^{125}I source spectrum, 465 angles per octant) and 0.4 min/spatial point (23 × 29 spatial cells, ^{192}Ir spectrum, 120 angles per octant) on our SGI RS10000 workstation. The same times are 0.02 min/spatial point for ^{125}I and 0.1 min/spatial point for ^{192}Ir when GAM-42 is used. We note that the much shorter times required for the GAM-42 calculations are due to the smaller number of energy groups used in the simulation.

At the conclusion of each DANTSYS calculation, the DANTSYS EDIT module was employed to convert the flux distribution to kerma by using the corresponding group kerma factors included in each library. Normalization factors were derived and applied to each TWODANT calculation using an automated procedure[15] to normalize the absolute kerma distributions to the same units assumed in the Monte Carlo simulations.

The DANTSYS results are obtained in the form of a two-dimensional array of values for the water-kerma rate at each point of the r-z geometry as determined by the code input. To obtain the kerma rate at points not coinciding with any of the DANTSYS grid points, a bilinear interpolation procedure has been implemented. To provide sufficient accuracy of the linear interpolates, the line source geometry factor $G(r,\theta)$, as defined by the American Association of Physicists in Medicine task group 43 (Ref. 29), was used to suppress spatial flux variations due to inverse square law. The geometry factor $G(r,\theta)$ for a line source of active length L at a point having polar coordinates (r,θ) is defined as (see Fig. 2)

$$G(r,\theta) = \begin{cases} \dfrac{\Delta\theta}{L \cdot r \cdot \sin\theta} & \theta \neq 0 \\ \dfrac{1}{r^2 - L^2/4} & \theta = 0 \end{cases} , \qquad (2)$$

where $\Delta\theta$ is the angle subtended by the active source with respect to the point (r,θ) and L coincides with the source region height as defined in Sec. II.A.

II.D. Monte Carlo Calculations

We have used a continuous-energy MCPT code[2,17–20] to evaluate the water kerma at various points in the cylindrical water phantoms discussed in Sec. II.A. The coherent and incoherent scattering together with

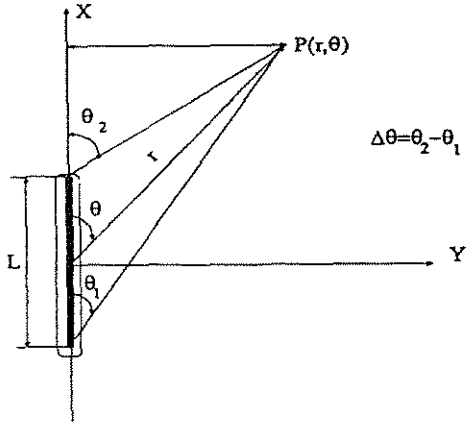

Fig. 2. Geometry representation of the quantities used for the geometry factor calculation Eq. (2) in a case of line source of active length L.

the photoeffect have been modeled in our simulations. Both the bounded next flight estimator[17] and once-more-collided-flux estimator[20] have been used for scoring. The scoring spheres surrounding each estimator point have been chosen to have diameters of <0.2 mfp in water. The kerma at 27 estimator points was evaluated by each MCPT run. Between 3 500 000 and 25 000 000 histories have been analyzed in each case, resulting in CPU time from 22 to 50 min/estimator point on the SGI RS10000 workstation used for all calculations. The water-kerma rate estimate standard deviation achieved has been between 0.4% and 2.25% within the 10-cm distance from the source center. Hubbell and Seltzer[30] mass-energy absorption coefficients were used to convert the scalar energy fluence into the collision kerma. It is well known that for photon energies below 800 keV, secondary electron equilibrium is approximately realized.[31,32] Under most conditions, e.g., excluding detectors immediately adjacent to media interfaces, absorbed dose is accurately approximated by kerma.[32] As bremsstrahlung production in water for this photon energy range is negligible, mass-energy absorption coefficients are essentially equivalent to the heating cross sections as derived by the NJOY code. All Monte Carlo results have been normalized to kerma per disintegration within the source in units cGy/mCi·h customarily used in clinical practice.[a]

Our MCPT simulations are rigorous benchmarks for assessing the accuracy of DANTSYS water-kerma calculations. However, as this code uses point-kerma estimators that do not exploit the cylindrical symmetry of our problem, calculating dose to an equivalent DANTSYS grid of points leads to extremely large CPU times. Thus, the efficiency comparisons with DANTSYS become meaningless. For evaluating DANTSYS efficiency, we have benchmarked DANTSYS against the DOSRZ EGS4 user code.[33] This is a Monte Carlo code in cylindrical *r-z* geometry, which was used with the same number and volumes of grid cells as in DANTSYS calculations. The EGS4 calculations scored the energy deposited in each region with no variance reduction techniques applied. Secondary electron transport was suppressed to avoid unnecessary calculations. For each geometry, the number of histories was selected in such a way to achieve a maximum standard deviation of ~2% or less over 99% of a 20-cm-diam × 20-cm-high scoring grid.

III. RESULTS AND DISCUSSION

Figure 3 shows the water-kerma radial distributions calculated by MCPT and DANTSYS with both the GAM-42 and G-210 multigroup libraries for ^{125}I and ^{192}Ir polychromatic spectra in the homogeneous water phantom. The differences between the two radionuclides show that (a) higher-energy sources are generally capable of delivering larger dose rates in bigger volumes and (b) lower-energy sources allow better dose localization and provide better conditions for shielding of sensitive tissues. Figure 3 shows that the DANTSYS and MCPT results closely agree and that the agreement is better when G-210 is used for the DANTSYS calculations relative to GAM-42.

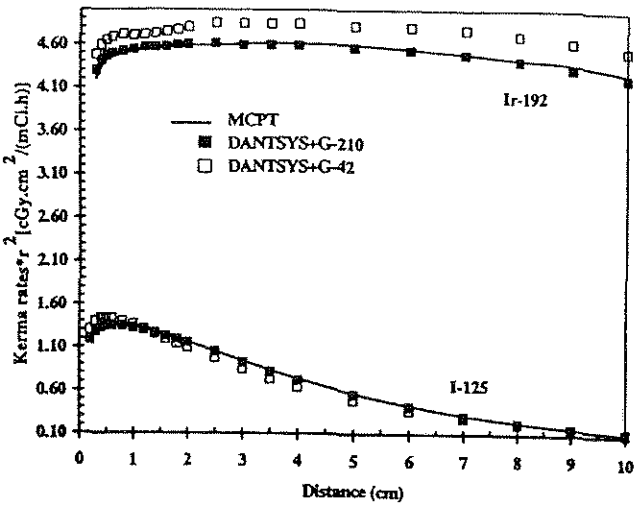

Fig. 3. Calculated water-kerma distributions in the homogeneous water phantom due to photon sources with polychromatic spectra of ^{125}I and ^{192}Ir. The MCPT calculations (curves) and DANTSYS calculations (symbols) with both the GAM-42 and G-210 multigroup libraries. The estimation points are distributed along the transverse source plane, with distances measured from the center of the source volume.

For quantitative analysis of the DANTSYS accuracy, two methods were used to evaluate the differences between the DANTSYS and MCPT water-kerma rate results. The graphical method is illustrated by Fig. 4, which shows the ratio of water kerma calculated by DANTSYS relative to that calculated by MCPT as a function of distance from the source center for ^{125}I, 100 keV, ^{192}Ir, and ^{137}Cs sources in the homogeneous water phantom using the GAM-42 library. Figures 5 and 6 show the same with the only difference being that Fe and Pb shields, respectively, with thicknesses of 1 and 2 mfp, depending on the photon source energy are present around the source. In addition, DANTSYS accuracy relative to the MCPT simulations is quantified by the root mean square error (rms):

$$\text{rms}\ (\%) = \sqrt{\frac{1}{N}\sum_{k=1}^{N}\left[1 - \frac{K_W^{DANT}(r_k)}{K_W^{MCPT}(r_k)}\right]^2} \times 100\ , \quad (3)$$

where $K_W^{DANT}(r_k)$ is the DANTSYS-calculated water kerma at position r_k and $K_W^{MCPT}(r_k)$ is the corresponding

[a]The transformation factor to the corresponding SI units is 1 cGy/mCi·h = 7.508 × 10^{-14} Gy/Bq·s.

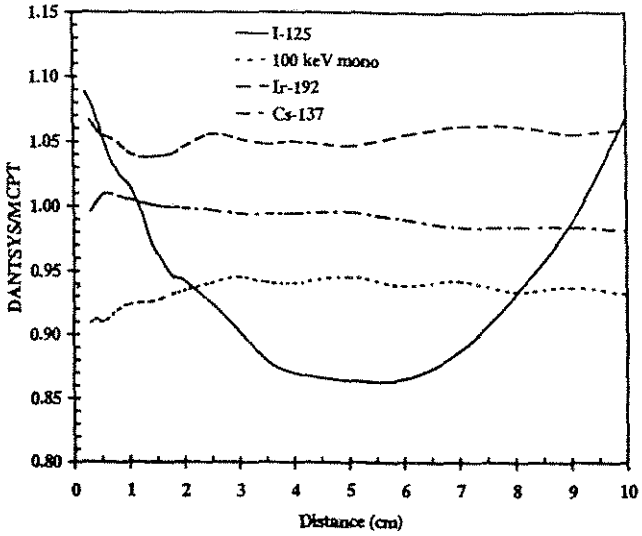

Fig. 4. DANTSYS results for the water kerma relative to MCPT, GAM-42 multigroup library, and homogeneous water phantoms. Sources are with spectral distributions of ^{125}I, 100 keV monoenergetic, ^{192}Ir, and ^{137}Cs.

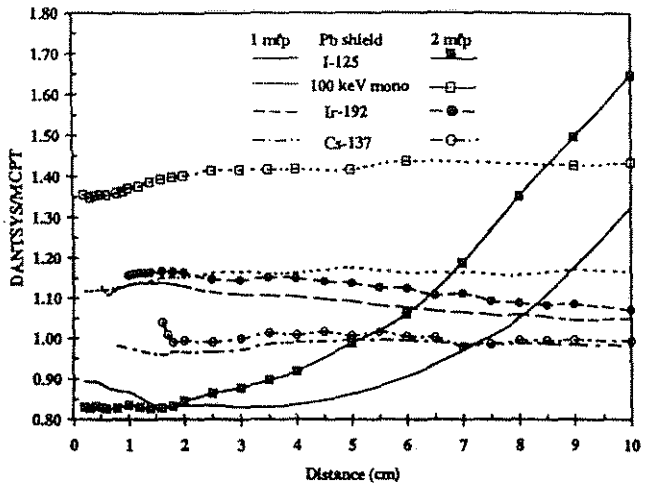

Fig. 6. DANTSYS results for the water kerma relative to MCPT, GAM-42 multigroup library, and Pb shields of thickness 1 mfp (thin curves) and 2 mfp (curves with symbols), respectively. Sources are with spectral distributions of ^{125}I, 100 keV monoenergetic, ^{192}Ir, and ^{137}Cs.

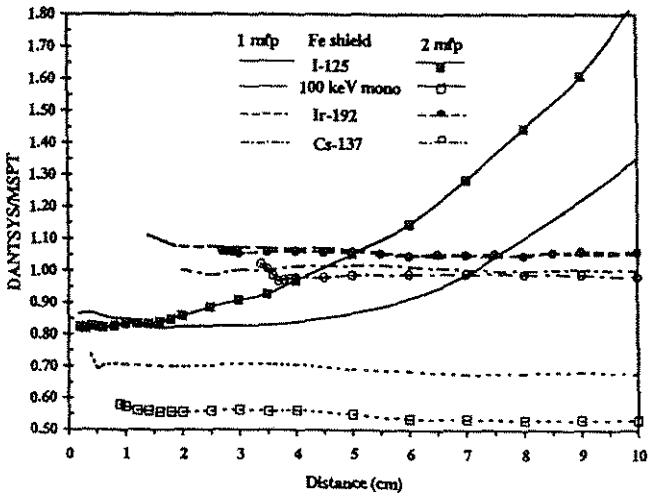

Fig. 5. DANTSYS results for the water kerma relative to MCPT, GAM-42 multigroup library, and Fe shields of thickness 1 mfp (curves) and 2 mfp (curves with symbols), respectively. Sources are with spectral distributions of ^{125}I, 100 keV monoenergetic, ^{192}Ir, and ^{137}Cs.

MCPT value. The rms error is tabulated in Table III at ~20 points for each case.

The results in Figs. 4, 5, and 6 and Table III demonstrate some of the problems specific to the studied energy range. For homogeneous water phantoms (Fig. 4), the discrepancies produced are generally >5% and clearly exceed 3 σ of the Monte Carlo results for all source spectral distributions except for ^{137}Cs, with even larger discrepancies for lower source energies. Figures 5 and 6 show that the consistency between DANTSYS and MCPT worsens when higher-atomic-number materials are introduced into the system. For ^{125}I, DANTSYS overestimates the dose by 30 to 88% at distances exceeding 3 to 4 mfp when shielding is introduced. DANTSYS underestimates the dose for the 100-keV monoenergetic spectral distribution by up to 45% for Fe. The dose overestimation for a 100-keV spectrum in the presence of the Pb shield is partly due to the primary photon energy and lead *K*-edge falling in the same energy group, as is discussed separately later. For the ^{192}Ir source, DANTSYS gives rise to a moderate dose calculation error of 6 to 16%. Only for ^{137}Cs is acceptable accuracy consistently achieved.

The rms errors of the discrete ordinates introduced by using GAM-42 show similar trends (Table III). The rms deviation decreases with increasing energy; is smaller for uniform spectra compared to discrete spectra, as defined in Sec. II.A; increases with the atomic number of the shielding material; and increases with the thickness of the shielding filter present in the system.

Table III shows that replacing the uniform 30- to 45-keV spectrum with a 30- to 45-keV spectrum having distribution proportional to E^2 (corresponding to the GAM-42 weighting function) in the MCPT simulations fails to improve the DANTSYS/GAM-42 accuracy.

Table III shows that the DANTSYS errors are particularly large for 75- to 100-keV sources (coinciding with the 35th GAM-42 group) in the presence of Pb shielding. This phenomenon was not observed with any other material and can be explained by the presence of the lead *K*-edge (88 keV) in this group. At 88 keV, the lead total

TABLE III

The rms Values of DANTSYS with GAM-42 Water Kerma Results Relative to MCPT Calculations*

Source Type	Water	Ti		Fe		Pb	
		1 mfp	2 mfp	1 mfp	2 mfp	1 mfp	2 mfp
^{125}I	7.98	16.4	26.9	16.6	28.2	15.2	23.6
30 keV to 45 keV	6.14	2.28	7.49	2.27	10.7	3.07	13.1
30 keV to 45 keV E^2	2.70	7.04	18.6	8.32	22.1	9.80	23.6
87 keV	---	---	---	---	---	77.3	94.4
75 keV to 100 keV	0.89	3.09	4.62	5.40	2.10	51.8	84.8
100 keV	7.11	24.5	35.5	30.3	44.9	14.8	39.1
200 keV to 300 keV	1.18	---	---	2.47	1.95	11.0	23.3
^{192}Ir	5.20	---	---	6.82	5.67	10.4	13.8
600 keV	6.41	---	---	5.53	12.1	16.1	25.6
^{137}Cs	0.89	---	---	1.00	1.84	2.90	1.34
600 keV to 700 keV	1.87	---	---	1.77	1.41	1.24	2.19

*The rms values are in percentage points.

macroscopic cross section discontinuously changes from 21.7 to 87.3 cm^{-1}. The straightforward procedure employed by NJOY for evaluating the multigroup constants, together with the weighting function used, does not account for such discontinuities. The resultant cross section, when averaged over the group, overestimates the true cross-section value for each energy below the edge while underestimating its value above the edge. The effect is stronger the larger the cross-section change at the edge energy. This explains why DANTSYS overestimates photon attenuation at 100 keV (above the *K*-edge) and underestimates that for 87-keV photons (just below the *K*-edge).

The results suggest that the GAM-42 library does not adequately represent the behavior of the cross section at low photon energies. We hypothesize that a major cause for this is that the weighting function used for GAM-42 development inadequately represents the flux spectrum characteristic of low-energy photon sources. As a result GAM-42 introduces distinct systematic errors depending on the actual energy photon flux distribution at each given point of the modeled system. This suggests that for a successful and accurate discrete ordinates method implementation in brachytherapy, multigroup libraries specially developed for brachytherapy applications are needed.

To verify this hypothesis, we have created a multigroup cross-section library with a very fine energy bin structure (G-210) and have recalculated all cases previously described. Figures 7, 8, and 9 are equivalent to Figs. 4, 5, and 6, with the only difference being that G-210 was used instead of GAM-42 for the DANTSYS calculations. Similarly, Table IV is equivalent to Table III but contains the rms deviations of the DANTSYS calculations relative to the MCPT results using G-210.

The figures show that for all cases considered, DANTSYS with G-210 cross sections computes the water kerma in very good agreement with our MCPT results. The maximum discrepancy is always <5%. As expected, good results are obtained regardless of the photon spectra used for this study. Unlike the GAM-42 calculations, the G-210 DANTSYS results are much less affected by the atomic numbers of the materials present in the system. The accuracy relative to MCPT is generally not sensitive to the thickness of the shielding materials, and the overall

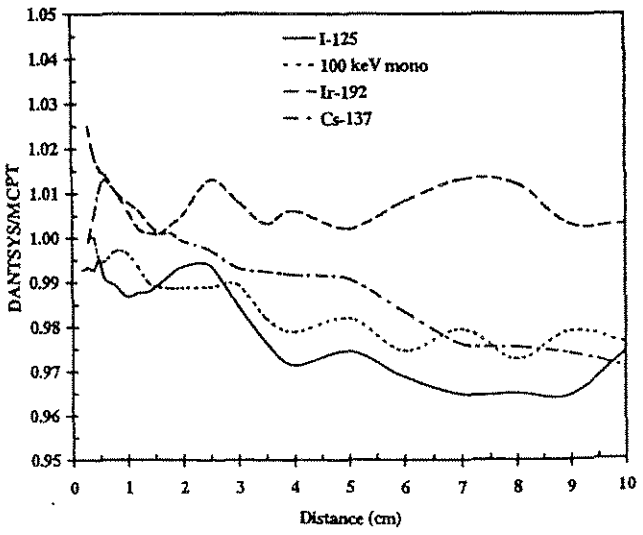

Fig. 7. DANTSYS results for the water kerma relative to MCPT, G-210 multigroup library, and homogeneous water phantoms. Sources are with spectral distributions of ^{125}I, 100 keV monoenergetic, ^{192}Ir, and ^{137}Cs.

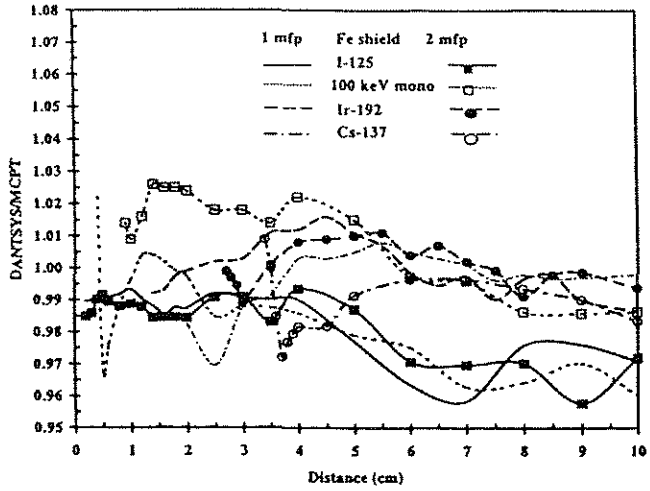

Fig. 8. DANTSYS results for the water kerma relative to MCPT, G-210 multigroup library, and Fe shields of thickness 1 mfp (curves) and 2 mfp (curves with symbols), respectively. Sources are with spectral distributions of ^{125}I, 100 keV monoenergetic, ^{192}Ir, and ^{137}Cs.

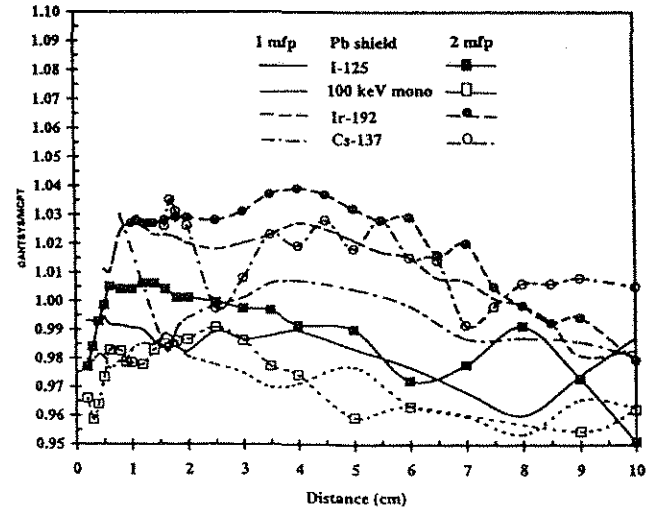

Fig. 9. DANTSYS results for the water kerma relative to MCPT, G-210 multigroup library, and Pb shields of thickness 1 mfp (curves) and 2 mfp (curves with symbols), respectively. Sources are with spectral distributions of ^{125}I, 100 keV monoenergetic, ^{192}Ir, and ^{137}Cs.

agreement is $<3\sigma$ of the Monte Carlo dose calculations for all distances studied. Similar conclusions can be drawn from the analysis of the data included in Table IV. All rms values have magnitudes <3%, which indicates the excellent agreement between the DANTSYS and Monte Carlo kerma calculations.

Only for the uniform 75- to 100-keV spectrum with a Pb shield is the rms deviation (Table IV) even moderately large and reaches 6% relative to MCPT. Since the monoenergetic cases with 100- and 87-keV photon energies are not affected, we conclude that the *K*-edge discontinuity causes errors only for photons with energies within the group containing the edge. The comparison with the GAM-42 results shows that narrowing the energy group width mitigates this influence. However, the somewhat larger discrepancy indicates the need for specific treatment of the edge discontinuity to provide adequate multigroup cross-section constants.

We used DANTSYS with the G-210 multigroup library to assess its accuracy for off-the-transverse-plane calculations. Figure 10 shows the accuracy of DANTSYS relative to the MCPT water-kerma rate results as a function of angle with respect to the positive *z*-axis direction in the homogeneous water phantoms and sources with spectral distributions of ^{125}I, 100 keV monoenergetic, ^{192}Ir, and ^{137}Cs, with scatter-to-primary dose ratios (SPR), listed in Figs. 10 and 11. Larger SPR values required smaller aspect ratios, leading to a larger number of spatial mesh cells and higher-order angular quadrature sets for adequate accuracy. We have obtained the results in Fig. 10 using 66 × 52 mesh cells (12:1 aspect ratio) for ^{125}I, while 28 × 26 (25:1 aspect ratio) sufficed for ^{137}Cs. The results clearly indicate that the DANTSYS calculations agree closely with the MCPT simulations. The maximal discrepancy is <2% except for the case of ^{125}I, where it is 3% at an angle of 9 deg. The somewhat larger discrepancy at 0 deg for ^{192}Ir and 100-keV spectra is due to the poor statistical precision of DANTSYS' Monte Carlo uncollided flux estimate at the source longitudinal axis (30 versus 1% σ on the transverse axis). Taking into account the small sizes of the sources modeled, the number of primary photon trajectories intersecting the spatial mesh cells along the *z*-axis is small, which leads to poor statistics. The results also indicate that large statistical uncertainties in the uncollided flux estimate may affect the accuracy for cases with both small and large SPRs. Therefore, care must be taken to achieve a sufficiently accurate uncollided flux estimate to avoid unnecessary decreases in accuracy.

Figure 11 illustrates the accuracy of DANTSYS in duplicating off-axis dose distributions for sources shielded by 1 mfp of Fe. Because of the larger cross-section magnitudes and correspondingly smaller mfp length in Fe, finer spatial mesh cells were required to obtain an appropriate finite difference geometry representation. For energies >100 keV, incoherent and coherent scattering together constitute >45% of the total cross section, resulting in larger SPRs. As a result, smaller aspect ratios and correspondingly higher-order angular quadratures must be used. The comparison shown in Fig. 11 clearly demonstrates the excellent consistency between the DANTSYS and MCPT calculations. The maximal discrepancy observed is ~3% at 0 deg in the case of ^{125}I and at 45 deg in the case of ^{137}Cs. The large 6% difference observed in the case of ^{192}Ir with a 1.31-cm Fe shield

TABLE IV

The rms Values of DANTSYS with G-210 Water Kerma Results Relative to MCPT Calculations*

Source Type	Water	Ti		Fe		Pb	
		1 mfp	2 mfp	1 mfp	2 mfp	1 mfp	2 mfp
^{125}I	2.00	2.05	2.00	1.81	1.90	1.69	1.60
30 keV to 45 keV	1.34	1.99	2.21	2.59	2.64	2.50	1.89
30 keV to 45 keV E^2	1.24	2.29	2.91	1.79	2.17	2.30	2.95
87 keV	---	---	---	---	---	1.68	2.45
75 keV to 100 keV	1.71	2.42	2.13	1.41	1.54	3.81	6.05
100 keV	1.50	1.15	2.24	2.15	1.75	2.60	2.74
200 keV to 300 keV	1.05	---	---	2.22	1.49	1.68	1.72
^{192}Ir	0.96	---	---	0.76	0.64	1.89	2.63
600 keV	0.84	---	---	2.22	0.95	2.02	1.70
^{137}Cs	1.33	---	---	1.01	1.52	1.29	1.92
600 keV to 700 keV	1.59	---	---	1.03	1.18	1.57	0.95

*The rms values are in percentage points.

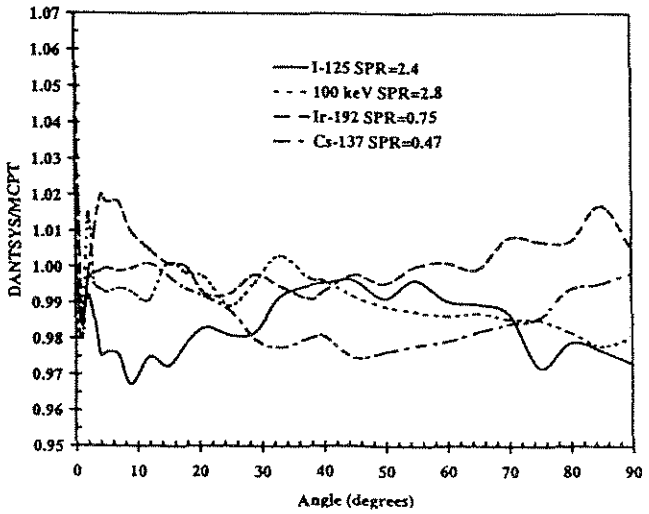

Fig. 10. Comparison of the polar kerma distribution results of DANTSYS relative to MCPT at a 5.0-cm distance from the source center in the homogeneous water phantom, G-210 multigroup library. Spectral distributions are of ^{125}I, 100 keV monoenergetic, ^{192}Ir, and ^{137}Cs. SPR denotes the scatter-to-primary ratio at 0 deg in each case as calculated by MCPT.

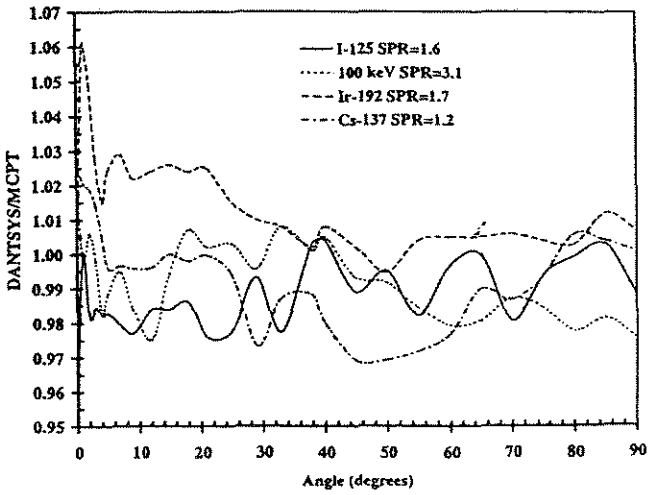

Fig. 11. Comparison of the polar kerma distribution results of DANTSYS relative to MCPT at a 5.0-cm distance from the source center in the homogeneous water phantom, G-210 multigroup library. Spectral distributions are of ^{125}I, 100 keV monoenergetic, ^{192}Ir, and ^{137}Cs. SPR denotes the scatter-to-primary ratio at 0 deg in each case as calculated by MCPT. An Fe shield of thickness of 1 mfp is present around the source.

at 1 deg is, as in the homogeneous case, due to a poorly calculated uncollided flux and corresponding primary kerma rate. The conclusions made in the case of a 1-mfp Fe shield are in general valid for all other materials and thicknesses studied.

Table V compares the CPU run times of the DANTSYS and EGS4 simulations for equivalent geometries on an RS10000 processor. On average, DANTSYS is between two and five times faster than EGS4, with efficiency improving for lower energies. Except for ^{125}I, the introduction of a 1-mfp Fe shield did not lead to a noticeable increase in DANTSYS efficiency relative to EGS4 since the increased number of required EGS4 histories has been largely compensated for by the large number of spatial mesh cells needed by DANTSYS. The somewhat smaller DANTSYS efficiency in the case of 100 keV with a 1-mfp Fe shield demonstrates the fact that the optimal spatial mesh is difficult to select a priori.

TABLE V

Computational Details of EGS4/DOSRZ and DANTSYS Calculations for the Cases of ^{125}I, 100 keV Monochromatic, ^{192}Ir, and ^{137}Cs Spectral Distributions for Homogeneous and 1-mfp Fe Shield Assemblies*

	EGS4/DOSRZ Results			DANTSYS Results			
Source Spectral Distribution	Number of Histories (in millions)	Maximum Standard Deviation Percent in 99% of Volume	CPU Time (min)	Number of Mesh Cells (Regions)	Quadrature Number of Angles per Octant	CPU Time (min)	DANTSYS/ DOSRZ CPU Time
Homogeneous case							
^{125}I	160	1.78	295	2067	210	59	0.20
100 keV	50	1.51	320	2067	210	64	0.20
^{192}Ir	40	1.90	247	1479	210	66	0.27
^{137}Cs	12	1.19	38	264	210	17	0.44
1-mfp Fe shield							
^{125}I	400	2.25	360	2456	210	55	0.15
100 keV	61	1.95	178	1666	325	132	0.74
^{192}Ir	55	1.50	221	1204	210	70	0.32
^{137}Cs	36	2.66	96	930	210	45	0.47

*All CPU times provided are valid on RS10000 Silicon Graphics workstation.

The analysis of the DANTSYS simulations with both the GAM-42 and G-210 cross-section libraries shows that DANTSYS with the G-210 results is much less sensitive to the particular shape of the "true" flux spectrum throughout the modeled system and is essentially "spectrum independent" for brachytherapy calculations. Increasing the number of energy groups, however, requires further refinement of the spatial mesh size as well as higher orders of angular quadrature to achieve accurate results. As the group widths become increasingly narrow, the individual groups appear increasingly "black" (i.e., absorbing) since most scattering results in downscatter out of the group. Satisfying these requirements along with the larger number of energy groups leads to highly intensive computations and makes three-dimensional calculations problematic with commonly available computational resources.

A straightforward way to increase the discrete ordinates method computational efficiency is to reduce the number of phase-space cells. One way of achieving this reduction is to develop suitable multigroup libraries with a broader energy bin structure. A comparison between the GAM-42 and G-210 DANTSYS simulations shows a gain in efficiency easily exceeding a factor of 10. The gain is due not only to a smaller number of groups but also to relaxing the other requirements for the calculations such as the number of spatial mesh cells and the order of angular quadrature set used. However, broadening the energy groups will require implementation of suitable weighting functions to achieve the desired accuracy. Appropriate procedures for handling the *K*-edge discontinuities together with accounting for characteristic X-ray contributions are also critical for derivation of adequate multigroup cross-section libraries with a minimum number of energy groups.

The use of higher-order spatial-differencing schemes and/or adaptive mesh refinement techniques might allow the use of significantly larger spatial mesh sizes, and also correspondingly smaller angular quadrature orders, thus relaxing the computer resources requirements and speeding up the computations even with a large number of energy groups. Both approaches potentially lead to a smaller number of spatial mesh cells and correspondingly lower-order angular quadratures, thus significantly reducing the computational time.

IV. CONCLUSIONS

This study shows that the discrete ordinates method in general and the DANTSYS code system in particular can accurately model water-kerma rate distributions arising from photon spectra and source geometries typical of brachytherapy. However, achieving a high (<5%) level accuracy over a large range of brachytherapy problem geometries and spectra has proven to be a challenging task and requires careful specifications of the following operational parameters:

1. *The choice of appropriate multigroup library:* The G-210 fine-energy-group library indeed allows accuracy

equivalent to that of a continuous-energy MCPT code. However, the large number of groups significantly increases the CPU time and the other computational resources and does not adequately increase computational efficiency. The development of optimal multigroup libraries containing a small number of groups, and being specifically designed for brachytherapy applications is of primary importance. This certainly includes a development of suitable procedures for adequate treatment of atomic electron shell discontinuities in the photoeffect interactions.

2. *Mitigation of ray effects:* The DANTSYS internal ray-tracing first-collision source option adequately mitigates ray effects but in general requires a relatively large fraction of the overall DANTSYS CPU times.

The results show that a P_3 Legendre polynomial expansion provides sufficient angular approximation of the photon scattering for all the energies and material studied.

The small source sizes also dictate the need for a relatively large number of spatial mesh cells (and correspondingly higher-order angular quadratures) to be used for adequate geometry representation. The results presented here indicate that angular quadratures containing 210 angles per octant (S_{40}) or less are sufficient to achieve satisfactory accuracy within 5% of the corresponding MCPT simulations.

The results presented here are not optimized for computational efficiency but are intended only to establish accuracy. The preliminary comparison with the EGS4 Monte Carlo code shows that a gain in efficiency of a factor from 2 to 5 is nevertheless achievable. However, this gain is not sufficient to enable the use of discrete ordinates codes in treatment planning. Future efforts directed toward reducing the number of phase-space cells used in the calculations as well as optimizing the other necessary features (such as the implementation of appropriate ray effects mitigation techniques) hopefully would create the necessary grounds for a successful and efficient discrete ordinates application to brachytherapy.

ACKNOWLEDGMENT

This study has been supported in part by the National Institutes of Health grant R01 CA46640.

REFERENCES

1. J. F. WILLIAMSON, "Recent Development in Basic Brachytherapy Physics," *Medical Radiology: Radiation Therapy Physics*, p. 247, R. A. SMITH, Ed., Springer-Verlag, Berlin, Germany (1995).

2. J. F. WILLIAMSON, H. PERERA, and Z. LI, "Comparison of Calculated and Measured Heterogeneity Correction Factors for ^{125}I, ^{137}Cs, and ^{192}Ir Brachytherapy Sources near Localized Heterogeneities," *Med. Phys.*, **20**, 209 (1993).

3. J. F. WILLIAMSON, "The Sievert Integral Revisited: Evaluation and Extension to ^{125}I, ^{169}Yb, and ^{137}Cs Brachytherapy Sources," *Int. J. Rad. Oncol. Biol. Phys.*, **36**, 1239 (1996).

4. W. F. MILLER, Jr., and E. E. LEWIS, *Computational Methods of Neutron Transport*, John Wiley & Sons, New York (1984).

5. F. J. MUCKENTHALER, L. B. HOLLAND, and J. L. HILL, "Measurements for the Three-Dimensional Oak Ridge Transport Code Verification Experiment," ORNL/TM-9528, Oak Ridge National Laboratory (1985).

6. W. A. RHOADES, R. L. CHILDS, M. B. EMMETT, and S. N. CRAMER, "Applications of the Three-Dimensional Oak Ridge Code," *Proc. Topl. Mtg. Reactor Physics and Shielding*, Chicago, Illinois, September 17–19, 1984, p. 225, American Nuclear Society (1984).

7. K. D. LATHROP, "Discrete Ordinates Methods for the Numerical Solution of the Transport Equation," *Reactor Technol.*, **15**, 107 (1975).

8. Y. HARIMA and S. TANAKA, "A Study of Buildup Factors, Angular and Energy Distributions at Small Distances from Three Source Geometries—Plane Isotropic, Point Isotropic, and Plane Normal—for Low-Energy Gamma-Ray Incidence on Water," *Nucl. Sci. Eng.*, **90**, 165 (1985).

9. H. HIRAYAMA, S. TANAKA, Y. SAKAMOTO, K. V. SUBBAIAH, and Y. HARIMA, "Comparison of Gamma-Ray Point Isotropic Buildup Factors Including Fluorescence and Bremsstrahlung in Lead Using Discrete Ordinates and Point Monte Carlo Methods," *J. Nucl. Sci. Technol.*, **27**, 524 (1990).

10. S. KITSOS, A. ASSAD, C. M. DIOP, and J. C. NIMAL, "Determination of Point Isotropic Buildup Factors of Gamma Rays Including Incoherent and Coherent Scattering for Aluminum, Iron, Lead, and Water by the Discrete Ordinates Method," *Nucl. Sci. Eng.*, **117**, 47 (1994).

11. S. KITSOS, C. M. DIOP, A. ASSAD, and J. C. NIMAL, "Improvement of Gamma-Ray S_n Transport Calculations Including Coherent and Incoherent Scatterings and Secondary Sources of Bremsstrahlung and Fluorescence: Determination of Gamma-Ray Buildup Factors," *Nucl. Sci. Eng.*, **123**, 215 (1996).

12. R. T. SANTORO, R. G. ALSMILLER, Jr., J. M. BARNES, G. T. CHAPMAN, and J. S. TANG, "Comparison of Measured and Calculated Neutron and Gamma Ray Energy Spectra Behind an In-Line Shielded Duct," *J. Fusion Energy*, **2**, 403 (1982).

13. H. HANDA, K. HAYASHI, and H. NARITA, "Radiation Streaming Analysis of Screw Duct," *8th Int. Conf. Radiation Shielding*, Arlington, Texas, April 24–28, 1994, p. 918, American Nuclear Society (1994).

14. N. SASAMOTO and K. TAKEUCHI, "Analysis of ^{60}Co Gamma-Ray Transport Through Air by Discrete-Ordinates Transport Codes," *Nucl. Technol.*, **47**, 189 (1980).

15. G. M. DASKALOV, R. S. BAKER, R. C. LITTLE, D. W. O. ROGERS, and J. F. WILLIAMSON, "Multigroup Discrete Ordinates Photon Transport Calculations of Water Kerma for Brachytherapy Applications," *Proc. Topl. Conf. Radiation Protection and Shielding*, Nashville, Tennessee, April 19–23, 1998, p. 261, American Nuclear Society (1998).

16. R. E. ALCOUFFE, R. S. BAKER, F. W. BRINKLEY, D. R. MARR, R. D. O'DELL, and W. F. WALTERS, "DANTSYS: A Diffusion Accelerated Neutral Particle Transport Code System," LA-12969-M, Los Alamos National Laboratory, June 1995.

17. J. F. WILLIAMSON, "Monte Carlo Evaluation of Kerma at a Point for Photon Transport Problems," *Med. Phys.*, **14**, 567 (1987).

18. Z. LI and J. F. WILLIAMSON, "Volume-Based Geometric Modeling for Radiation Transport Calculations," *Med. Phys.*, **19**, 667 (1992).

19. J. F. WILLIAMSON and A. S. MEIGOONI, "Quantitative Dosimetry Methods for Brachytherapy," *Brachytherapy Physics*, J. F. WILLIAMSON, B. T. THOMADSEN, and R. NATH, Eds., p. 87, Medical Physics Publishing Company, Madison, Wisconsin (1995).

20. Z. LI, J. F. WILLIAMSON, and H. PERERA, "Monte Carlo Calculation of Kerma-to-a-Point in the Vicinity of Media Interfaces," *Phys. Med. Biol.*, **38**, 1825 (1993).

21. *A Handbook of Radioactivity Measurements Procedures*, 2nd ed., NCRP Report No. 58, National Council of Radiation Protection and Measurements, Washington, D.C. (1985).

22. G. P. GLASGOW and L. T. DILLMAN, "Specific γ-Ray Constant and Exposure Rate Constant of ^{192}Ir," *Med. Phys.*, **6**, 49 (1979).

23. D. E. CULLEN, M. H. CHENG, J. H. HUBBELL, S. F. PERKINS, E. F. PLECHATY, J. A. RATHKOPF, and J. H. SCOFIELD, "Tables and Graphs of Photon Interaction Cross Sections from 10 eV to 100 GeV Derived from LLNL Evaluated Nuclear Data Library (ENDL)," UCRL-50400, Vol. 6, Rev. 4, Lawrence Livermore National Laboratory (1989).

24. "HUGO-VI: Photon Interaction Data in ENDF/B-VI Format," RSIC Data Library DLC-146, Oak Ridge National Laboratory (Aug. 1989).

25. R. E. MacFARLANE and D. W. MUIR, "The NJOY Nuclear Data Processing System Version 91," LA-12740-M (Oct. 1994); see also RSIC Code Package PSR-355, Oak Ridge National Laboratory (Dec. 1996).

26. R. E. ALCOUFFE, "An Adaptive Weighted Diamond-Differencing Method for Three-Dimensional *XYZ* Geometry," *Trans. Am. Nucl. Soc.*, **68A**, 206 (1993).

27. R. E. ALCOUFFE, "Diffusion Synthetic Acceleration Methods for the Diamond-Difference Discrete-Ordinates Equations," *Nucl. Sci. Eng.*, **64**, 344 (1977).

28. R. S. BAKER, "A Stochastic First Collision Source for TWODANT," *Proc. 8th Int. Conf. Radiation Shielding*, Arlington, Texas, April 24–28, 1994, Vol. 1, p. 926, American Nuclear Society (1994).

29. R. NATH, L. L. ANDERSON, G. LUXTON, K. A. WEAVER, J. F. WILLIAMSON, and A. S. MEIGOONI, "Dosimetry of Interstitial Brachytherapy Sources: Recommendations of the AAPM Radiation Committee Task Group No. 43," *Med. Phys.*, **22**, 209 (1995).

30. J. H. HUBBELL and S. M. SELTZER, "Tables of X-Ray Mass Attenuation Coefficients and Mass Energy-Absorption Coefficients 1 keV to 20 keV for Elements $Z = 1$ to 92 and 48 Additional Substances of Dosimetric Interest," *NISTIR* 5632 (May 1995).

31. H. E. JOHNS and J. R. CUMMINGHAM, *The Physics of Radiotherapy*, 4th ed., Chap. 7, pp. 220–224, Charles C. Thomas, Publisher, Springfield, Illinois (1983).

32. R. K. VALICENTI, A. S. KIROV, A. S. MEIGOONI, V. MISHRA, R. K. DAS, and J. F. WILLIAMSON, "Experimental Validation of Monte Carlo Dose Calculations About a High-Intensity Ir-192 Source for Pulsed Dose-Rate Brachytherapy," *Med. Phys.*, **22**, 821 (1995).

33. W. R. NELSON, A. HIRAYAMA, and D. W. O. ROGERS, "The EGS4 Code System," SLAC-265, Stanford Linear Accelerator Center (1985).